energies

MDPI

Article

Research on the Thermal Aging Characteristics of Crosslinked Polyethylene Cables Based on Polarization and Depolarization Current Measurement

Yamei Li [1], Zhaowei Peng [1], Dangguo Xu [1], Shiyang Huang [1], Yanfeng Gao [1] and Yuan Li [2,*]

[1] Electric Power Research Institute, State Grid Jibei Electric Power Co., Ltd., Beijing 100054, China
[2] College of Electrical Engineering, Sichuan University, Chengdu 610065, China
* Correspondence: hvliyuan@scu.edu.cn

Abstract: Although XLPE cables are widely used in power transmission and distribution systems, their insulating properties are susceptible to degradation due to thermal aging. In order to clarify the influence law of the thermal aging process on the structural and dielectric properties of XLPE cables, this paper investigates the thermal aging characteristics of XLPE cables by using polarization and depolarization current measurement. Results show that when the XLPE cable is aged at 140 °C, the crystallinity of the insulation layer appears to increase and then decrease. With the increase in aging time, micron-sized microvoids appear on the surface of the XLPE. At the same time, the DC conductivity and 0.1 Hz dielectric loss factor of the insulating layer increase with the aging time. The average DC conductivity increased from 2.26×10^{-16} S/m for new cables to 4.47×10^{-16} S/m after aging for 432 h, while the dielectric loss increased from 0.11% to 0.42%. The polarization characteristics of thermal-aged cables were further analyzed using the extended Debye model. Results indicate that the time constant of the third branch of the model increased significantly with increasing aging time. A correspondence between this parameter and the thermal aging time of the cable was established. Thermal aging can damage the crystalline structure of XLPE, so that the number of interfaces between the crystalline and amorphous regions of the material increases, resulting in structural damages and a decline in the dielectric properties of the cable insulation.

Keywords: XLPE cable; polarization and depolarization current; thermal aging; extended Debye model

Citation: Li, Y.; Peng, Z.; Xu, D.; Huang, S.; Gao, Y.; Li, Y. Research on the Thermal Aging Characteristics of Crosslinked Polyethylene Cables Based on Polarization and Depolarization Current Measurement. *Energies* **2024**, *17*, 2274. https://doi.org/10.3390/en17102274

Academic Editor: Ayman El-Hag

Received: 25 March 2024
Revised: 23 April 2024
Accepted: 2 May 2024
Published: 9 May 2024

1. Introduction

Crosslinked polyethylene (XLPE) cables are widely used in urban distribution networks [1]. However, under long-term high-temperature operating conditions, the XLPE insulation material of power cables will inevitably undergo thermal aging, leading to deterioration in electrical, mechanical, and thermal performance, and even cable failures [2–4]. Since thermal aging often occurs throughout the entire cable, it may cause a decrease in the performance of the entire cable line, and ultimately lead to multiple points of breakdown [5]. Therefore, a timely and accurate detection of the thermal aging degree of the cable is crucial for the safe and stable operation of the power system.

The polarization and depolarization current (PDC) measurement has been increasingly applied in the evaluation of the insulation condition in recent years due to its advantages of fewer measurement modules, lightweight equipment, lower cost, and shorter measurement time [6–8]. Researchers have extracted various diagnostic parameters such as the polarization current, aging factor, PDC slope, relationship between the depolarization current and time, DC conductivity and its non-linear coefficient, 0.1 Hz dielectric loss and its non-linear coefficient, etc., from PDC measurement results, to diagnose the insulation condition of cables [9–12]. These parameters can reflect the overall electrical performance of the cable. However, there has been limited research on how to use PDC measurement

results to determine the thermal aging degree of cables. It is worth noting that according to the extended Debye theory, the dielectric process of thermal-aged cables can usually be equivalent to a three-branch model, with each branch representing different polarization and depolarization types [13]. Thermal aging will cause changes in the PDC characteristics of the cable, leading to changes in the branch parameters of the extended Debye model [14]. If the information reflecting the degree of thermal aging of the cable can be separated from the extended Debye model, the accuracy of insulation diagnoses for thermal-aged cables can be greatly improved. However, it is still unclear what the correlation is between the three-branch parameters of the extended Debye model of thermal-aged cables and the degree of thermal aging. Meanwhile, the physical mechanism of thermal-aging-induced changes in XLPE dielectric properties also lacks sufficient investigations.

To address the aforementioned issues, this study artificially prepared short cable samples with different durations of thermal aging, and conducted PDC measurement on the samples. The variations of the cable DC conductivity, dielectric loss factor, and other parameters with thermal aging time were analyzed. The corresponding relationship between Debye model branch parameters and cable thermal aging time was determined. Additionally, differential scanning calorimetry (DSC) testing and scanning electron microscopy (SEM) testing were employed to analyze the influence of thermal aging duration on the structural parameters of XLPE insulation materials, based on which the physical mechanism of the changes in dielectric parameters of XLPE materials caused by thermal aging was analyzed from the perspective of the aggregated structure of XLPE.

2. Materials and Methods

To conduct research on the thermal aging characteristics of cables, samples of short cables with different degrees of thermal aging were first prepared. These short cable samples were cut from XLPE long cables with a model of YJV22-3×95, rated at 8.7/10 kV. Each short cable sample was 50 cm long, as illustrated in Figure 1. A total of 25 short cable samples were cut. Subsequently, the short cable samples were divided into five groups, G0, G1, G2, G3, and G4, with each group containing five cables. The short cable samples in groups G1, G2, G3, and G4 were placed in an oven for thermal aging, with aging temperatures set at 140 °C and aging durations of 108 h, 216 h, 324 h, and 432 h, respectively. The short cable samples in group G0 were not subjected to thermal aging and served as the control group for new cables.

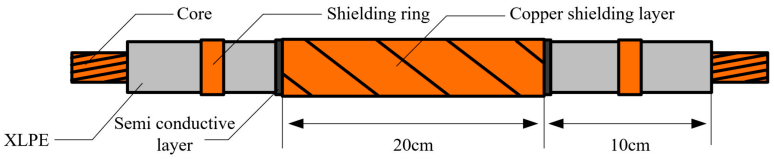

Figure 1. The schematic of the thermal aging XLPE cable samples.

After the thermal aging, PDC measurements were performed on the short cable samples, with the platform shown in Figure 2. The DC power supply used was the ZGF-120 DC high-voltage generator, with an output DC voltage range of 0–5 kV, voltage ripple coefficient less than 0.1%, and maximum output current of 20 mA. The cable core was connected to the DC high-voltage generator, while the copper tape was connected to the ammeter current input port. Additionally, a shielding ring was added and grounded on the exposed insulation layer at both ends of the cable to avoid the influence of the surface current on the PDC measurement results. During the measurement, the switch S was toggled to positions S1 and S2 to measure the polarization current i_{pol} and depolarization current i_{depol} of the sample, respectively. The measurement voltage was set at 1 kV, with polarization and depolarization times both set to 90 s.

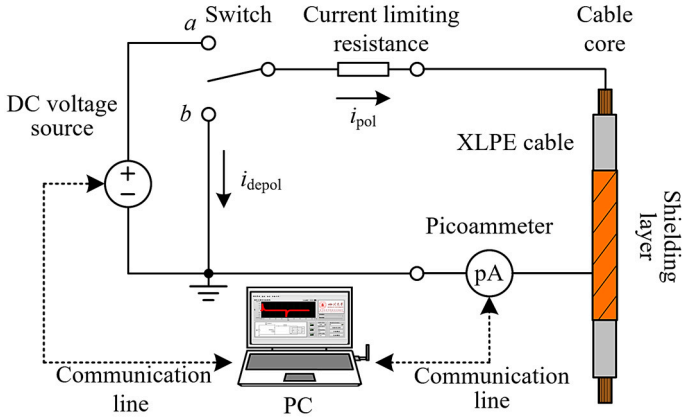

Figure 2. Schematic of cable PDC measurement platform.

To comprehensively understand the changes in the mechanical properties and microstructure of samples before and after thermal aging, this study sliced the thermal-aged samples and conducted differential scanning calorimetry (DSC) tests and scanning electron microscopy (SEM) observations on the samples.

The DSC test can reflect the material's elastic modulus [15]. Before DSC testing, the semiconductor layers on both sides of the aged samples were removed to prevent other materials from mixing into the XLPE. Afterwards, the samples were cut into small pieces, with individual sample weights ranging from 3 mg to 8 mg. The cut block samples were placed in crucibles, with nitrogen gas being introduced into the entire testing environment as a protective gas. The samples were heated according to the programmed heating rate and temperature (30~140 °C, with a heating rate of 10 °C/min), during which the thermal flow changes in the sliced samples were recorded.

The SEM test can reflect the material's microstructure [16]. Before SEM testing, liquid nitrogen was used to quench the samples. The quenched sample surfaces were then gold-sputtered and observed under the SEM. The SEM testing instrument used in this experiment was the JSM-7500F scanning electron microscope, with an acceleration voltage range of 0.1 kV to 30 kV, an adjustable resolution range of 1.0 nm (15 kV) to 1.4 nm (1 kV), and an adjustable magnification range of 25 to 800,000 times. Since the cable samples underwent overall thermal aging, the observation area could be randomly selected.

3. Extraction Method of Electrical Parameters Based on PDC

PDC measurement can reflect various polarization and relaxation information inside the measured material. Based on the current obtained from the measurement, parameters such as the conductivity, dielectric loss factor, etc., can be calculated. Additionally, an extended Debye model reflecting the polarization type of the material can be constructed.

3.1. Extraction of Conventional Electrical Parameters

After applying a step voltage excitation to the cable, various electrical conduction and polarization processes begin within the XLPE insulation of the cable. This is the response of the insulation to the step voltage excitation applied, which can be manifested as a polarization current response. Since the capacitive current component decays rapidly, the influence of the capacitive current will be neglected in investigating the polarization process. At this point, the polarization current is mainly composed of the absorption current and conduction current.

The absorption current component is related to the polarizability of the insulating material of the cable. After applying an external electric field, the current response density $J(t)$ within the insulation can be expressed as

$$J(t) = \sigma E(t) + \frac{\mathrm{d}D(t)}{\mathrm{d}t} \quad (1)$$

In Equation (1), σ represents the conductivity of the insulating material; $E(t)$ is the electric field strength applied to the material; and $D(t)$ is the electric induction intensity of the material.

If the insulation layer of an XLPE cable is isotropic, the induced electric field strength inside the insulation when an external electric field is applied is related to the applied electric field strength and the polarization strength of the insulation material, as

$$D(t) = \varepsilon_0 \varepsilon_\infty E(t) + \Delta P(t) \tag{2}$$

In the equation, ε_0 represents the vacuum permittivity; ε_∞ is the relative dielectric constant of the insulating material at optical frequencies; and $\Delta P(t)$ is the rate of change of the polarization intensity of the material, which can be represented as

$$\Delta P(t) = \varepsilon_0 \int_0^\infty f(t-\tau) E(\tau) \mathrm{d}\tau \tag{3}$$

where $f(t)$ represents the dielectric response function of the insulating material.

Therefore, the current response density $J(t)$ can be expressed as follows:

$$J(t) = \sigma E(t) + \varepsilon_0 \varepsilon_\infty \frac{\mathrm{d}E(t)}{\mathrm{d}t} + \varepsilon_0 \frac{\mathrm{d}}{\mathrm{d}t} \int_0^t f(t-\tau) E(\tau) \mathrm{d}\tau \tag{4}$$

The three components on the right side of Equation (4) are the conductive current density, the capacitive current density, and the absorption current density, respectively. When the insulating material is in a planar structure, the polarization process is characterized by the polarization current flowing through the interior of the material:

$$i_{\mathrm{pol}}(t) = C_0 \left[\frac{\sigma}{\varepsilon_0} U(t) + \varepsilon_\infty \frac{\mathrm{d}U(t)}{\mathrm{d}t} + \frac{\mathrm{d}}{\mathrm{d}t} \int_0^t f(t-\tau) U(\tau) \mathrm{d}\tau \right] \tag{5}$$

where $U(t)$ represents the applied voltage.

Since an XLPE cable is of a coaxial structure, its geometric capacitance can be expressed as

$$C_0 = \frac{2\pi \varepsilon_0 L}{\ln[D_{\mathrm{i}}/D_{\mathrm{c}}]} \tag{6}$$

In the equation, D_{i} represents the outer diameter of the cable insulation layer; L represents the cable length; and D_{C} represents the inner diameter of the cable insulation layer.

Due to the rapid decay of the capacitive current, it is often ignored. The polarized current after ignoring the capacitive current can be expressed as follows:

$$i_{\mathrm{pol}} \approx C_0 U_0 \left[\frac{\sigma}{\varepsilon_0} + f(t) \right] \tag{7}$$

In the equation, U_0 represents the constant polarization voltage. Similarly, the depolarization current can be expressed as follows:

$$i_{\mathrm{depol}} = C_0 U_0 [f(t) - f(t + t_c)] \tag{8}$$

where t_{c} represents the polarization time.

Based on Equations (7) and (8), the conductivity of XLPE cable insulation can be inferred as

$$\sigma = \frac{\varepsilon_0 \left(i_{\mathrm{pol}} - i_{\mathrm{depol}} \right)}{C_0 U_0} \tag{9}$$

On the other hand, due to the limited information contained in the time-domain signal results measured by the PDC, it is necessary to perform a frequency-domain diagnosis of

XLPE cable insulation aging. The current signal measured by the PDC can be transformed from the time domain to the frequency domain, typically using the Fourier transform, with the following specific method:

$$\begin{aligned}\dot{I}(\omega) &= C_0\dot{U}(\omega)\left[\tfrac{\sigma}{\varepsilon_0} + \mathrm{j}\omega\left(\varepsilon_\infty + \dot{X}'(\omega) - \mathrm{j}\omega X''(\omega)\right)\right] \\ &= \mathrm{j}\omega C_0\dot{U}(\omega)\left[\varepsilon_\infty + X'(\omega) - \mathrm{j}\left(\tfrac{\sigma_0}{\varepsilon_0\omega} + X''(\omega)\right)\right] \\ &= \mathrm{j}\omega C_0\dot{U}(\omega)\left[\varepsilon'(\omega) - \mathrm{j}\varepsilon''(\omega)\right]\end{aligned} \tag{10}$$

Equation (10) can also be expressed as

$$\dot{I}(\omega) = \mathrm{j}\omega\dot{U}(\omega)\left[C'(\omega) - \mathrm{j}C''(\omega)\right] \tag{11}$$

According to the definition of the dielectric loss factor, the dielectric loss factor of insulation materials can be calculated by the following equation:

$$\tan\sigma(\omega) = \frac{I_R(\omega)}{I_C(\omega)} = \frac{C''(\omega)}{C'(\omega)} = \frac{\varepsilon''(\omega)}{\varepsilon'(\omega)} = \frac{\frac{\sigma}{\varepsilon_0\omega}}{\varepsilon_\infty + X'(\omega)} + \frac{X''(\omega)}{\varepsilon_\infty + X'(\omega)} \tag{12}$$

In the equation, $I_R(\omega)$ is the frequency domain expression of the resistive current, where $I_R(\omega) = \omega UC'(\omega)$; $I_C(\omega)$ is the frequency domain expression of the capacitive current, where $I_C(\omega) = j\omega UC''(\omega)$; C' is the real part of complex capacitance; C'' is the imaginary part of complex capacitance; and ε' and ε'' are the real and imaginary parts of the complex dielectric constant, respectively. It is worth mentioning that in the expressions of $I_R(\omega)$ and $I_C(\omega)$, $U(\omega)$ represents the frequency domain expression of the applied voltage signal, which is generally considered a step signal due to the high resistance of the XLPE cable.

3.2. Extraction of Extended Debye Model Branch Parameters

Dielectric molecules will undergo polarization under the action of an electric field. On the one hand, the positive and negative charge centers of the dielectric molecules will separate, forming electric dipoles. The orientation and distribution of electric dipoles vary with the variation of the electric field, thereby affecting the dielectric constant and other electrical properties of the dielectric molecules. On the other hand, when the dielectric molecules undergoes aging, there may be interfaces between structures with different degrees of aging [17]. After applying an external DC electric field to the dielectric molecules, the electric fields on both sides of the interface transition from capacitive distribution to resistive distribution, during which charges accumulate at the interface, triggering the interface polarization process. Different dielectric structures or material types can correspond to different polarization processes, the dynamic characteristics of which can be described by the extended Debye model. Therefore, the extended Debye model is an effective method for studying the phenomenon of dielectric aging [18–21].

The extended Debye model mainly consists of three parts: the resistance branch corresponding to the resistance value of the dielectric molecules, the capacitance branch corresponding to the geometric capacitance of the dielectric molecules, and multiple *RC* series branches, corresponding to different polarization processes within the dielectric molecules [21]. The model is shown in Figure 3.

In Figure 3, R_0 represents the insulation resistance of the dielectric molecules; in other words, this branch corresponds to the conductivity process inside the dielectric molecules. The current flowing through R_0 is the conductance current during polarization. C_0 represents the geometric capacitance of the dielectric molecules, which corresponds to the capacitive charging process inside the dielectric molecules just after an externally applied DC voltage is applied to the dielectric molecules. The current flowing through C_0 is the capacitive current during polarization. And since the *RC* series branch corresponds to the polarization process, the current flowing through each *RC* series branch is the various types of polarization absorption currents.

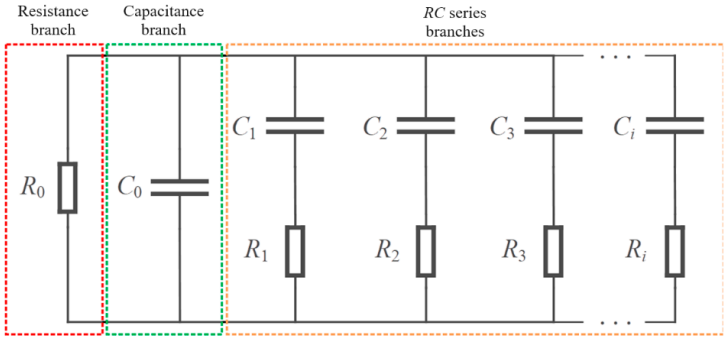

Figure 3. The extension of the Debye model equivalent circuit.

In the extended Debye model, the complex dielectric constant of the dielectric molecules is given by the following equation:

$$\varepsilon(\omega) = \varepsilon_\infty + \sum_{i=1}^{n} \frac{\varepsilon_s - \varepsilon_\infty}{1 + j\omega\tau_i} \tag{13}$$

Among which ε_s represents the dielectric constant of the dielectric molecules under the direct current voltage; ε_∞ represents the dielectric constant of the dielectric molecules under the optical frequency voltage; and n represents the various polarizations and processes that may occur in the dielectric molecules.

After removing the external electric field, the polarized structures in the dielectric molecules gradually relax. This is reflected in multiple parallelled *RC* series branches, where the discharge current of the capacitor C_i is formed, representing the depolarization current, which can be expressed by the following equation:

$$i_{depol} = \sum_{i=1}^{n} A_i e^{\frac{-t}{\tau_i}} \tag{14}$$

Therefore, solving the depolarization current curve can obtain the parameter values of each branch in the extended Debye model, and an electrical performance evaluation of XLPE insulation can be carried out.

4. Experimental Results

To study the changes in the mechanical properties and microstructure of the thermal-aged samples, physical and chemical property tests, as well as microscopic observations, were conducted on the samples of G0–G4 groups as described in the Section 2. Due to the consistent results of multiple cable samples under the same aging conditions, the subsequent PDC, DSC, and SEM analyses show only results of one cable. But the experimental results of crystallinity, DC conductivity, tan$\delta_{0.1}$, and branch parameters of the extended Debye model are the average value of five cable samples of each group to better display the trend of data changes.

4.1. Physicochemical and Microscopic Testing Results

4.1.1. DSC Testing

The crystallinity of cable samples was analyzed using DSC for both non-aged and the other four groups of thermal-aged samples. The DSC exothermic curves are shown in Figure 4.

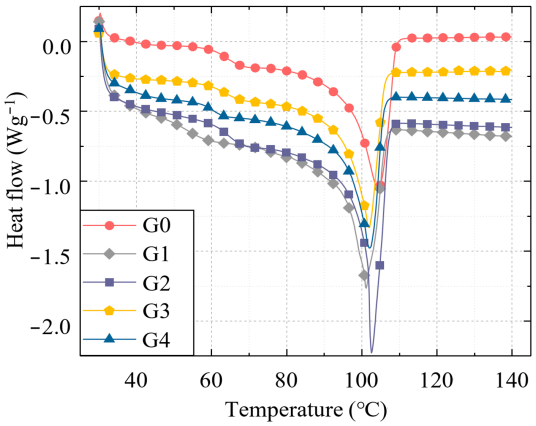

Figure 4. DSC exothermic curves of cable samples with different aging times.

After determining the DSC curve of the sample, the melting enthalpy ΔH_f of the crystalline part of the sample can be obtained by calculating the area enclosed by the sample melting peak curve and the baseline. By comparing this value with the melting enthalpy ΔH^*_f of the 100% crystallized sample, shown as Equation (15), the actual crystallinity of the sample can be obtained. The results are shown in Figure 5.

$$Crystallinity(\%) = \frac{\Delta H_f}{\Delta H_f^*} \times 100\% \quad (15)$$

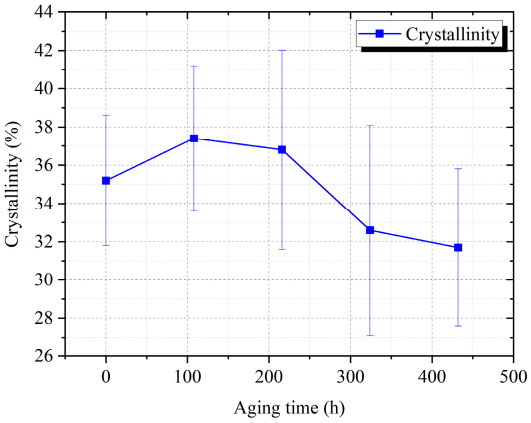

Figure 5. Average crystallinity of samples subjected to thermal aging at different aging times.

According to the results in Figure 5, with the increase in thermal aging time, the crystallinity of the samples shows a trend of first increasing and then decreasing. Before 108 h of thermal aging, the average crystallinity of the samples increased with aging time, from 35.2% of the unaged samples (G0 samples) to 37.4% at 108 h (G1 samples) of thermal aging. The increasement can be attributed to the fact that the XLPE material was in a stage of recrystallization in the early stage of thermal aging. Under the action of antioxidants, the chain scission oxidation process of XLPE molecules is inhibited, resulting in little or no thermal oxidative degradation of XLPE; at the same time, thermal aging causes incomplete crystals in the insulation to melt and recrystallize, with some amorphous regions transforming into crystalline regions, leading to an increase in crystallinity. With a further increase in thermal aging time, XLPE insulation continues to undergo thermal cracking, with molecular chains gradually breaking, entering the stage of thermal oxidative aging, and forming large numbers of chain scissions and oxidation–reduction products; at this time, the crystals in the XLPE insulation begin to transform into an amorphous state, and the crystallinity of the samples shows a decreasing trend.

4.1.2. SEM Testing

In order to characterize the microstructural changes in thermal-aged samples, SEM observations were conducted on G0 to G4 samples. The results are shown in Figure 6. According to the figures, during the thermal aging process, chain scission and crystalline melting within XLPE will occur, leading to the formation of microvoids in the samples. No microvoids were found on the fracture surfaces of the non-aged samples; after 108 h of thermal aging, a small number of microvoids began to appear, with the maximum size being approximately 1.3 μm. After 216 h of thermal aging, the maximum size of the microvoids in the samples increased to 1.9 μm. After 324 h of aging, the number of microvoids in the samples significantly increased, with the maximum size of the microvoids being approximately 2.0 μm. The size of microvoids increased to 2.1 μm after 432 h of aging, indicating a very severe level of degradation in the samples at this point.

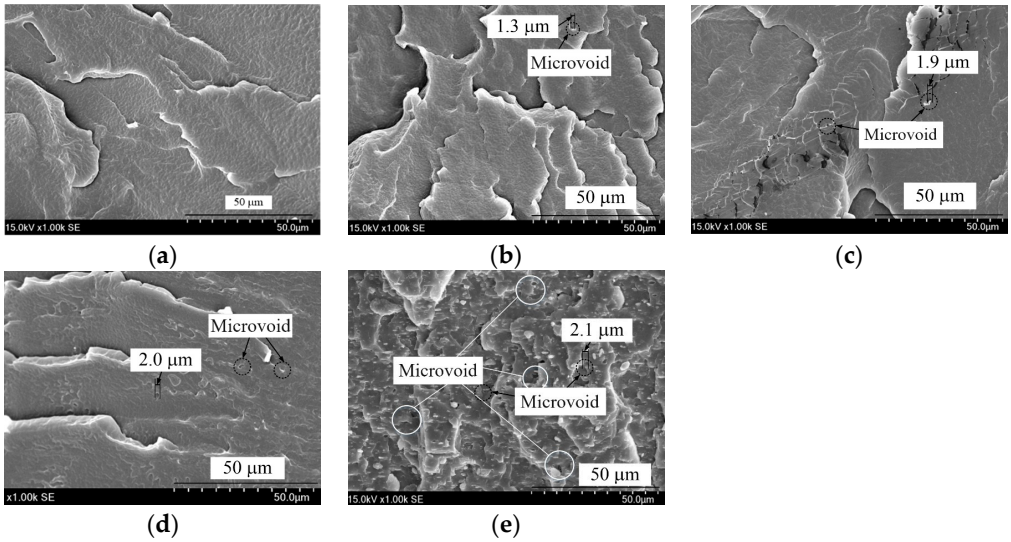

Figure 6. SEM results of samples subjected to thermal aging at different aging times—(**a**) 0 h; (**b**) 108 h; (**c**) 216 h; (**d**) 324 h; (**e**) 432 h.

4.2. PDC Measurement and Electrical Parameters' Extraction Results

In order to characterize the changes in dielectric properties of thermal-aged samples, PDC measurements (polarization voltage of 1 kV, polarization/depolarization time of 90 s) were conducted on the samples. The results are shown in Figure 7. Based on the polarization/depolarization current measurement data, the DC conductivity σ and the 0.1 Hz dielectric loss factor $\tan\delta_{0.1}$ of the samples can be calculated.

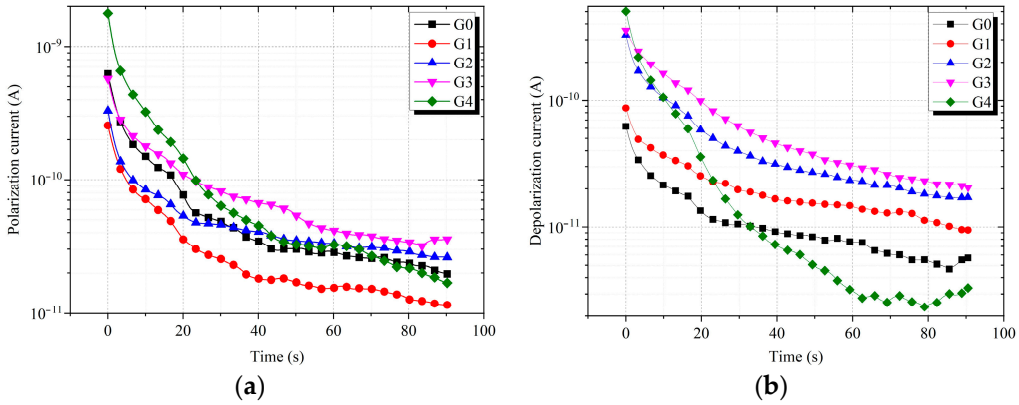

Figure 7. PDC measurement results of thermal-aged cables. (**a**) Polarization current; (**b**) depolarization current.

4.2.1. DC Conductivity σ

To characterize the conductivity of thermal-aged samples, the DC conductivity was calculated based on the PDC curves of the samples. The calculated results are shown in Figure 8. From the figure, it can be observed that the average DC conductivity of the thermal-aged samples changes relatively little compared to the unaged samples: the average DC conductivity of the unaged G0 samples is 2.26×10^{-16} S/m, while after 432 h of thermal aging (G4 samples), the value increases slightly to 4.47×10^{-16} S/m, with no significant order of magnitude change. It is analyzed that during thermal aging, the molecular chain segments in local areas of XLPE will first break and oxidize to form isolated micropores. As the thermal aging time increases, the number of isolated micropores in the material will continue to increase. However, due to the inability of charges to move freely between isolated micropores, the increase in DC conductivity of the thermal-aged samples is not substantial.

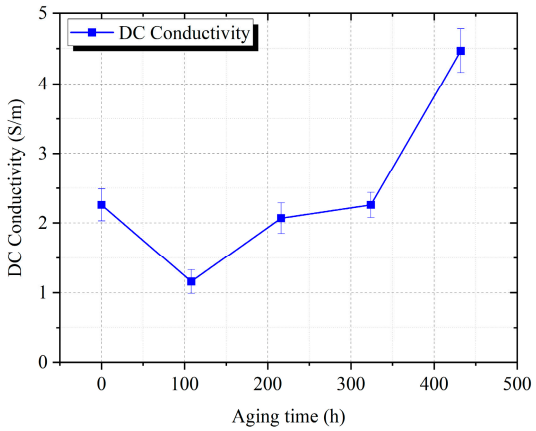

Figure 8. Average DC conductivity of thermal-aged cable samples.

In addition, with the aging time increasing, the DC conductivity of the sample first decreases and then increases. This is because of the recrystallization phenomenon in the early stage of thermal aging, which makes the existing crystal structure of the sample tend to be more compact, thus more effectively suppressing charge movement, leading to a decrease in the DC conductivity of the sample. As the thermal aging time increases, the crystal regions of the sample begin to be damaged again, and the DC conductivity of the sample gradually increases.

4.2.2. The 0.1 Hz Dielectric Loss Factor $\tan\delta_{0.1}$

The 0.1 Hz dielectric loss factor $\tan\delta_{0.1}$ calculated based on PDC results of thermal-aged samples is shown in Figure 9. According to the figure, as the aging time increases, the average $\tan\delta_{0.1}$ of the samples increases from 0.11% (G0 samples) to 0.19% (G1 samples), up to 0.42% (G4 samples) for the samples aged for 432 h. During this process, on one hand, polar groups such as carbonyl groups are generated due to thermal aging of the molecular chain segments, which will cause dipole polarization loss. On the other hand, material crystalline regions melt and form new interfaces such as a "crystal region–amorphous region", which will cause interface loss. With the increase in thermal aging time, the number of broken molecular chain segments in the sample increases, and more "crystal region–amorphous region" interfaces are generated, resulting in an increase in the $\tan\delta_{0.1}$ of the sample.

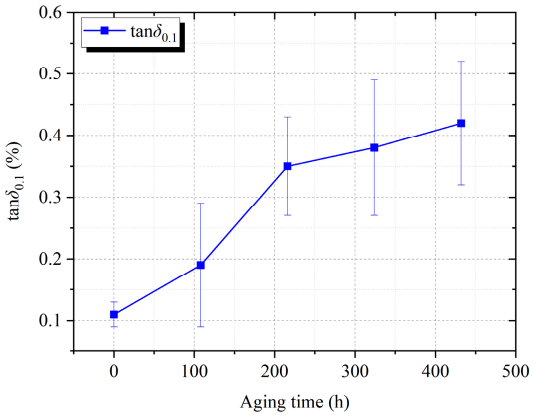

Figure 9. Average $\tan\delta_{0.1}$ of thermal-aged cable samples.

4.2.3. Branch Parameters of Extended Debye Model

The construction of the extended Debye model and the identification of branch parameters of the depolarization current for cable samples with different thermal aging times were carried out. The average branch time constant τ_i and fitting coefficient A_i after three-branch fitting are shown in Table 1. Here, notice that the τ_3 of the unaged sample is 93.76 s. With the deepening of the aging degree, τ_3 gradually increases to 129.23 s and 141.38 s, and finally 182.32 s after 432 h of aging, which is nearly twice that of the unaged sample. The first and second branch time constants of samples with different degrees of thermal aging, on the other hand, are close to those of the unaged sample.

Table 1. Branch parameters of extended Debye model for cables with different thermal aging times.

Aging Time	Fitting Order	A_1	τ_1 (s)	A_2	τ_2 (s)	A_3	τ_3 (s)
0 h	3	2.08×10^{-11}	1.07	2.82×10^{-11}	9.13	1.33×10^{-11}	93.76
108 h	3	2.93×10^{-11}	1.13	3.67×10^{-11}	12.75	2.12×10^{-11}	129.23
216 h	3	1.24×10^{-10}	1.16	1.71×10^{-10}	12.02	3.27×10^{-11}	141.38
324 h	3	7.25×10^{-11}	1.51	2.49×10^{-10}	15.16	3.54×10^{-11}	167.08
432 h	3	2.31×10^{-10}	1.44	2.70×10^{-10}	14.41	1.12×10^{-11}	182.32

Based on the above characteristics, we can conclude that τ_3 can best characterize the thermal aging degree of the samples. By plotting the curve of the relationship between aging time and τ_3 (as shown in Figure 10), and fitting it mathematically, the equation for assessing the degree of thermal aging of cables based on a can be obtained as

$$t = 63110.26 - 63591.30^{\tau_3} \quad (16)$$

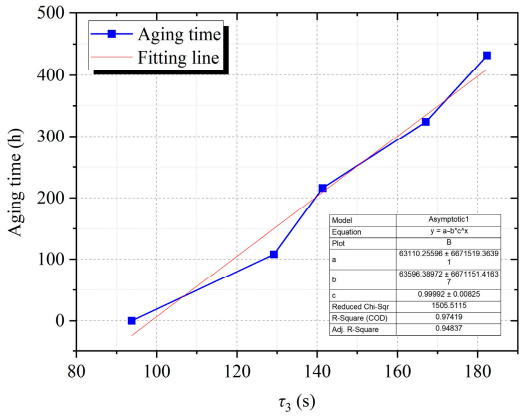

Figure 10. Relationship curve of aging time and τ_3.

Under high-temperature conditions, the XLPE material is subjected to thermal oxidation aging and thermal cracking, leading to its degradation. Thermal oxidation aging generates gas and solid decomposition products within the material, with gas decomposition products forming micrometer-scale micropores in localized decomposition zones, while solid decomposition products increase the polarization products in the sample, thereby increasing the time constant of the sample branch. The third branch mainly characterizes the interface polarization phenomenon at the "crystal region–amorphous region" interfaces in the material. From the variation law of τ_3 of the third branch, it can be observed that the rate of decrease in cable sample resistance induced by thermal aging is greater than the rate of increase in sample capacitance. This is manifested as an increase in the product of branch resistance R_3 and branch capacitance C_3, i.e., an increase in the time constant of the third branch.

5. Discussion

XLPE is a polymer composed of crystalline and amorphous regions, with the molecular chain segments in the amorphous region arranged in a random manner, while the molecular chain segments in the crystalline region are arranged in an ordered manner, as illustrated in Figure 11a. During thermal aging, localized thermal oxidative aging will occur in the amorphous region of XLPE material, leading to molecular chain breakage, and the broken molecular chain segments will be oxidized to form polar groups such as carbonyl groups. At the same time, due to the structural heterogeneity of the material itself, as well as the differences in density between the amorphous and crystalline regions, the material experiences uneven heating and aging during the thermal aging process.

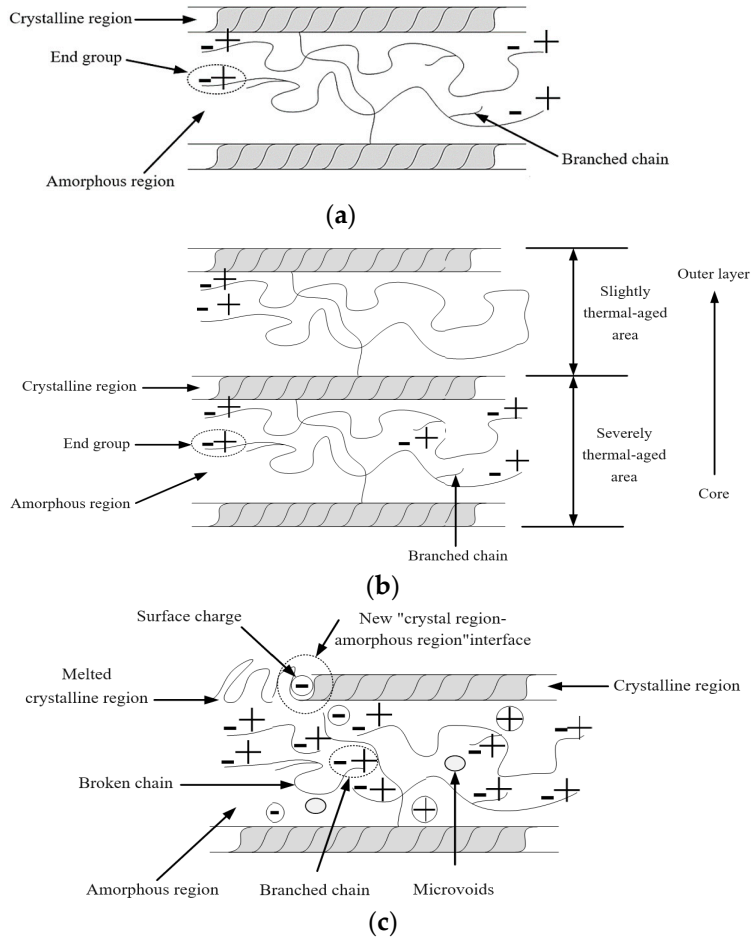

Figure 11. Microstructure and polarization changes within thermal-aged cable samples. (**a**) Unaged sample; (**b**) sample under uneven thermal aging; (**c**) polarizations within thermal-aged sample.

The unevenness of thermal aging is mainly manifested in two aspects: On one hand, the inner temperature of the operating cable is higher while the outer temperature is lower; thus, the insulation inside the cable is usually more severely thermal-aged, as illustrated in Figure 11b. On the other hand, due to the unevenness of the material structure, under high-temperature conditions, some crystalline regions in the material will melt and transform into amorphous regions, leading to the formation of more "crystal region–amorphous region" interfaces. Additionally, thermal-aging-induced material oxidation and material decomposition will also create micropore voids within the XLPE material, resulting in "void–XLPE" interfaces. Under the action of an electric field, these interfaces will undergo dipole polarization and interface polarization, as illustrated in Figure 11c.

During the thermal aging process, the sample will undergo molecular chain segment breakage and generate polar functional groups. In addition, new interfaces ("crystal region–amorphous region" interfaces, "air–XLPE" interface, etc.) will also be generated, which will cause an increase in the dipole polarization and interface polarization degree of the sample, resulting in an increase in the polarization current and depolarization current of the sample shown in Figure 7. In the figure, the polarization and depolarization curves of G4 samples have a larger slope, indicating more polar aging products and a severe degree of aging of the sample, therefore leading to a severe polarization process inside the insulation material of the cable. Meanwhile, the phenomenon of recrystallization, indicated by the results in Figure 5, causes the initial part of the polarization current to show a trend of first decreasing and then increasing with the thermal aging time (G0 to G4).

On the other hand, due to the absence of new charge migration pathways in the material, the increase in DC conductivity of the thermal-aged samples is not significant (as shown in Figure 8). In the early stage of thermal aging (before 108 h of aging), the oxidation process of XLPE molecular chains is inhibited by the antioxidant in the insulation material, preventing thermal oxidation degradation. At the same time, recrystallization phenomena gradually transform some amorphous regions into crystalline regions, resulting in a more regular arrangement of XLPE molecular chains and a decrease in the charge migration rate, leading to a decrease in DC conductivity in the early stage of thermal aging as aging progresses. Before 216 h of thermal aging of the cable samples, the DC conductivity is even lower than that of the samples that have not undergone thermal aging. With increasing thermal aging time, the crystal zones of the cable samples gradually deteriorate, leading to a gradual increase in DC conductivity.

In addition, the aging process is accompanied by molecular chain breakage and an increase in the number of interfaces, which will lead to a gradual increase in the loss factor $\tan\delta_{0.1}$. The formation of new interfaces can simultaneously create isolated microvoids within the XLPE, and as the aging time increases, the degree of interface polarization increases. Since isolated microvoids do not provide a channel for charge movement, the increase in sample conductivity is not significant with increasing aging time. However, aging will result in the formation of a large number of polar groups such as carbonyl groups, combined with the new interfaces, which will increase the dielectric constant and capacitance of the sample. The increase in capacitance is greater relative to the decrease in resistance, and the third time constant is the product of capacitance and resistance. This leads to an overall increase in the third time constant τ_3 of the sample with increasing aging time.

Also, it should be noted that for this study, as the experimental subjects used 8.7/10 kV AC cables, the conclusions regarding thermal aging mainly apply to this type of cable. For cables used under the DC voltage, although their dielectric loss factor and conductivity also tend to increase under thermal aging according to previous research, the amplitude of changes in dielectric parameters may vary due to different specific components of insulation materials. Meanwhile, when adopting the PDC method to study the dielectric properties of thermal-aged cable samples, it is necessary to use the DC voltage to effectively distinguish the polarization process and the conductivity process for a better analysis. Since the detected results, such as dielectric loss, conductivity, etc., belong to the intrinsic properties

of the material, the PDC result under the DC voltage can also reflect the insulation state of the AC cable samples after thermal aging.

In future research, we will refer to previous research methods and conduct X-ray diffraction and infrared absorption spectroscopy tests on samples of thermally aged cables, therefore establishing a deeper understanding of the interrelationship between the microstructure and the dielectric parameters of insulation materials for thermally aged cables, and to deepen our understanding of the thermal aging mechanism of power cables [22].

6. Conclusions

In this paper, the thermal aging characteristics and mechanisms of XLPE cables based on polarization–depolarization current measurement are investigated. Conclusions are drawn as follows:

During the thermal aging process, microvoids, melted crystalline regions, and increased dipole polarization will be formed in XLPE materials, leading to an increase in the polarization current and depolarization current with aging time.

The DC conductivity and 0.1 Hz dielectric loss factor of thermal-aged cable samples both show an overall increasing trend with the aging time. However, due to that, no new charge transfer channels are formed in the material during aging; the increase in conductivity of thermal-aged samples is not significant. Meanwhile, the aging process will generate interfaces within XLPE, leading to a gradual increase in the material's dielectric loss factor.

Thermal aging will cause the molecular chain segments of materials to break and generate new "crystal region–amorphous region" interfaces. Meanwhile, due to the isolation of most microvoids within the material, the movement of charges is restricted. The decrease in sample resistance is smaller than the increase in capacitance. Therefore, the third branch time constant of the material's extended Debye model will increase, and its magnitude can reflect the degree of thermal aging of the material.

Author Contributions: Data curation, Y.L. (Yamei Li) and Z.P.; funding acquisition, Y.G.; investigation, Y.L. (Yamei Li) and D.X.; methodology, Y.L. (Yuan Li) and D.X.; supervision, S.H. and D.X.; validation, Y.L. (Yuan Li); writing—original draft, Y.L. (Yamei Li); writing—review and editing, D.X. and Y.L. (Yuan Li). All authors have read and agreed to the published version of the manuscript.

Funding: This research was funded by National Key Research and Development Program of China grant number 2022YFE0102500.

Data Availability Statement: The raw data supporting the conclusions of this article will be made available by the authors on request.

Conflicts of Interest: Authors Yamei Li, Zhaowei Peng, Dangguo Xu, Shiyang Huang, Yanfeng Gao were employed by the company State Grid Jibei Electric Power Co., Ltd. The remaining authors declare that the research was conducted in the absence of any commercial or financial relationships that could be construed as a potential conflict of interest.

References

1. Sun, W.J.; Liu, X.J.; Yuan, L.J.; Xiao, H.; Lu, J.M. Regulating the structure of crosslinked polyethylene and its application in ultra-high voltage cables. *Polym. Eng. Sci.* **2023**, *64*, 496–505. [CrossRef]
2. Wang, Z.; Hu, Y.; Gui, Z.; Zong, R. Halogen-free flame retardation and silane crosslinking of polyethylenes. *Polym. Test* **2003**, *22*, 533–538. [CrossRef]
3. Fothergill, J.C.; Montanari, G.C.; Stevens, G.C.; Teyssedre, G.; Nilsson, U.H. Electrical, microstructural, physical and chemical characterization of HV XLPE cable peelings for an electrical aging diagnostic data base. *IEEE Trans. Dielectr. Electr. Insul.* **2003**, *10*, 514–527. [CrossRef]
4. Li, C.; Chu, Z.; Zhang, L.; Zhang, J.; Tao, J. Insulation aging diagnosis and defect location of crosslinked polyethylene cable in the distribution network based on radio frequency identification. *Mater. Express* **2023**, *13*, 1772–1781. [CrossRef]
5. Li, Z.; Dong, Y.; Wu, Y.; Meng, Z.; Song, P.; Zhu, M.; Li, X.; Du, B. Breakdown Performance Evaluation and Lifetime Prediction of XLPE Insulation in HVAC Cables. *Energies* **2024**, *17*, 1337. [CrossRef]
6. Lin, S.; Zhou, K.; Li, Y. A novel PDC system and tanδ calculation process for insulation diagnosis of submarine cables. *IEEE Trans. Dielectr. Electr. Insul.* **2024**, *31*, 145–150. [CrossRef]

7. Zhou, K.; Yuan, H.; Li, Y.; Li, M.Z.; Li, Z.R.; Lin, S.Y. Assessing aging status and type of xlpe cable insulation with a graphic approach based on PDC measurement. *IEEE Trans. Power Deliv.* **2022**, *37*, 5114–5123. [CrossRef]
8. Morsalin, S.; Phung, B.T. Dielectric response study of service-aged XLPE cable based on polarisation and depolarisation current method. *IEEE Trans. Dielectr. Electr. Insul.* **2020**, *27*, 58–66. [CrossRef]
9. Basu, D.; Gholizad, B.; Ross, R.; Gargari, S. Thermal aging-based degradation parameters determination for grid-aged oil paper insulation. *IEEE Trans. Dielectr. Electr. Insul.* **2023**, *30*, 734–743. [CrossRef]
10. Saha, T.K.; Purkait, P.; Muller, F. Deriving an equivalent circuit of transformers insulation for understanding the dielectric response measurements. *IEEE Trans. Power Deliv.* **2005**, *20*, 149–157. [CrossRef]
11. Yang, F.; Du, L.; Yang, L.; Wei, C.; Wang, Y.; Ran, L.; He, P. A Parameterization Approach for the Dielectric Response Model of Oil Paper Insulation Using FDS Measurements. *Energies* **2018**, *11*, 622. [CrossRef]
12. Fofana, I.; Hadjadj, Y. Electrical-Based Diagnostic Techniques for Assessing Insulation Condition in Aged Transformers. *Energies* **2016**, *9*, 679. [CrossRef]
13. Morsalin, S.; Sahoo, A.; Phung, B. Recovery voltage response of XLPE cables based on polarisation and depolarisation current measurements. *IET Gener. Transmiss. Distrib.* **2019**, *13*, 5533–5540. [CrossRef]
14. Yu, X.F.; Song, Z.J.; Chen, Z.X. Study on the time domain dielectric properties of oil-impregnated paper with non-uniform aging based on the modified Debye model. In Proceedings of the ICHVE, Chengdu, China, 19–22 September 2016; pp. 1–4.
15. Maciejewska, M.; Łastawiecka, E.; Grochowicz, M. Thermal Characterization of Crosslinked Polymeric Microspheres Bearing Thiol Groups Studied by TG/FTIR/DSC under Non-Oxidative Conditions. *Materials* **2024**, *17*, 1372. [CrossRef] [PubMed]
16. Wilkinson, A.J. Advances in SEM–based diffraction studies of defects and strains in semiconductors. *Microscopy* **2000**, *49*, 299–310. [CrossRef] [PubMed]
17. Puente-Córdova, J.G.; Luna-Martínez, J.F.; Mohamed-Noriega, N.; Miranda-Valdez, I.Y. Electrical Conduction Mechanisms in Ethyl Cellulose Films under DC and AC Electric Fields. *Polymers* **2024**, *16*, 628. [CrossRef] [PubMed]
18. Lv, H.K.; Lu, T.H.; Xiong, L.Q.; Zheng, X.G.; Huang, Y.Y.; Ying, M.L.; Cai, J.C.; Li, Z. Assessment of thermally aged XLPE insulation material under extreme operating temperatures. *Polym. Test.* **2020**, *88*, 106569. [CrossRef]
19. Morsalin, S.; Phung, B.T. Modeling of dielectric dissipation factor measurement for XLPE cable based on Davidson-Cole model. *IEEE Trans. Dielectr. Electr. Insul.* **2019**, *26*, 1018–1026. [CrossRef]
20. Morsalin, S.; Phung, B.T.; Danikas, M. Diagnostic challenges in dielectric loss assessment and interpretation: A review. *IET Sci. Meas. Technol.* **2019**, *13*, 767–782. [CrossRef]
21. Li, H.; Li, J.Y.; Ma, Y.X.; Yan, Q.M. Effects of thermal aging on the crystal structures of the XLPE cable insulating material at different temperatures. *Proc. CSEE* **2017**, *37*, 6740–6748.
22. Rizzo, P.; Baione, F.; Guerra, G.; Martinotto, L.; Albizzati, E. Polyethylene unit cell and crystallinity variations as a consequence of different cross-linking processes. *Macromolecules* **2001**, *34*, 5175–5179. [CrossRef]